Piperidine Adsorption on Hydrated α-Alumina (0001) Surface Studied by Vibrational Sum Frequency Generation Spectroscopy

Gang Ma, Dingfang Liu, and Heather C. Allen*

Department of Chemistry, The Ohio State University, 100 West 18th Avenue, Columbus, Ohio 43210

Received May 21, 2004. In Final Form: September 26, 2004

The adsorption of piperidine vapor on the hydrated alumina (α-Al_2O_3, corundum) (0001) surface was investigated using vibrational broad bandwidth and scanning sum frequency generation (SFG) spectroscopy. The interfacial vibrational signature in the C−H stretching region of piperidine at the alumina (0001) surface is shown to be a sensitive spectroscopic probe revealing the adsorption mechanism. The neat piperidine surface, aqueous piperidine surface, and aqueous piperidium chloride surface were also investigated in the C−H stretching region by SFG to establish vibrational reference frequencies. After piperidine adsorption, piperidine vapor was removed and piperidine was found to be chemisorbed onto the alumina (0001) surface through protonation by surface hydroxyl groups. The O−H stretching region of the alumina surface before and after piperidine adsorption was also investigated, and the results revealed the decrease of the surface number density of alumina surface hydroxyl groups.

Introduction

It is well known that the adsorption process of organic compounds from the gas phase to the solid mineral surface influences the migration and the fate of organic compounds in the environment.[1,2] α-Al_2O_3 is commonly used as a model metal oxide.[3−12] In addition to its importance in the area of catalysis, α-Al_2O_3 is a common constituent in the inorganic fraction of soils and in atmospheric particles. α-Al_2O_3 (corundum) is found in soil by inheritance from the parent rocks. It alters readily under surface conditions and yields other secondary minerals such as kaolinite, gibbsite, diaspore, zoisite, and sillimanite.[13,14] α-Al_2O_3 is also found in the mineral dust component of tropospheric aerosols. The amount of mineral dust emitted into the atmosphere is significant and has been estimated to be between 1000 and 3000 Tg per year.[15−20] Furthermore, α-Al_2O_3, as well as γ-Al_2O_3, is one of the main constituents of rocket fuel exhaust formed by solid rocket motors.[21,22] In recent years, there has been concern that these alumina particles may affect the stratospheric ozone layer.[23−26]

This study focuses on the adsorption of piperidine, a model volatile organic compound, from the gas-phase to the adsorbed-phase on the (0001) surface of single-crystal α-Al_2O_3. Previously, piperidine has been used as a model molecule to investigate the mechanism of the photocatalytic degradation of nitrogen-containing compounds in environmental pollution treatments.[27] There are two reasons to choose piperidine as the model molecule. First, piperidine is a secondary amine. Secondary amines are common organic pollutants due to their extensive use in the pharmaceutical, pesticide, and rubber industries.[28] Recently, removal of these compounds from the environ-

* Author to whom correspondence should be addressed. E-mail: allen@chemistry.ohio-state.edu.

(1) Stumm, W.; Morgan, J. J. *Aquatic Chemistry*, 3rd ed.; John Wiley and Sons: New York, 1996.
(2) *Pesticides in the soil environment: processes, impacts, and modeling*; Cheng, H. H., Ed.; The Soil Science Society of America, Inc.: Madison, Wisconsin, 1990.
(3) Goss, K.-U.; Eisenreich, S. J. *Environ. Sci. Technol.* **1996**, *30*, 2135−2142.
(4) Goss, K.-U.; Schwarzenbach, R. P. *Environ. Sci. Technol.* **1998**, *32*, 2025−2032.
(5) Goss, K.-U.; Schwarzenbach, R. P. *J. Colloid Interface Sci.* **2002**, *252*, 31−41.
(6) Eng, P. J.; Trainor, T. P.; Brown, G. E., Jr.; Waychunas, G. A.; Newville, M.; Sutton, S. R.; Rivers, M. L. *Science* **2000**, *288*, 1029−1033.
(7) Hass, K. C.; Schneider, W. F.; Curioni, A.; Andreoni, W. *Science* **1998**, *282*, 265−268.
(8) Withbrodt, J. M.; Hase, W. L.; Schlegel, H. B. *J. Phys. Chem. B* **1998**, *102*, 6539−3548.
(9) Alavi, S.; Sorescu, D. C.; Thompson, D. L. *J. Phys. Chem. B* **2003**, *107*, 186−195.
(10) Ahn, J.; Rabalais, J. W. *Surf. Sci.* **1997**, *388*, 121−131.
(11) Elam, J. W.; Nelson, C. E.; Tolbert, M. A.; George, S. M. *Surf. Sci.* **2000**, *450*, 64−77.
(12) Nelson, C. E.; Elam, J. W.; Cameron, M. A.; Tolbert, M. A.; George, S. M. *Surf. Sci.* **1998**, *416*, 341−353.
(13) Sparks, D. L. *Environmental Soil Chemistry*, 2nd ed.; Academic Press: San Diego, 2003.
(14) Hsu, P. H. Aluminum hydroxides and oxyhydroxides. In *Minerals in Soil Environments*; 2nd ed.; Dixon, J. B., Weed, S. B., Eds.; The Soil Science Society of America, Inc.: Madison, Wisconsin, 1989; p 1244.
(15) Tegen, I.; Fung, I. *J. Geophys. Res.* **1994**, *99*, 22897−22914.
(16) Tegen, I.; Harrison, S. P.; Kohfeld, K.; Prentice, I. C.; Coe, M.; Heimann, M. *J. Geophys. Res.* **2002**, *107*, 4576.
(17) Mahowald, N.; Kohfeld, K.; Hansson, M.; Balkanski, Y.; Harrison, S. P.; Prentice, I. C.; Schulz, M.; Rodhe, H. *J. Geophys. Res.* **1999**, *104*, 15895−15916.
(18) Ginoux, P.; Chin, M.; Tegen, I.; Prospero, J. M.; Holben, B.; Dubovik, O.; Lin, S.-J. *J. Geophys. Res.* **2001**, *106*, 20255−20273.
(19) Chin, M.; Ginoux, P.; Kinne, S.; Torres, O.; Holben, B. N.; Duncan, B. N.; Martin, R. V.; Logan, J. A.; Higurashi, A.; Nakajima, T. *J. Atmos. Sci.* **2002**, *59*, 461−483.
(20) Zender, C. S.; Bian, H.; Newman, D. *J. Geophys. Res.* **2003**, *108*, 4416.
(21) Turco, R. P.; Toon, O. B.; Whitten, R. C.; Cicerone, R. J. *Nature* **1982**, *298*, 830−832.
(22) Cofer, W. R., III; Winstead, E. L.; Key, L. E. *J. Propul. Power* **1989**, *5*, 674−677.
(23) Molina, M. J.; Molina, L. T.; Zhang, R.; Meads, R. F.; Spencer, D. D. *Geophys. Res. Lett.* **1997**, *24*, 1619−1622.
(24) Danilin, M. Y.; Ko, M. K. W.; Weisenstein, D. K. *J. Geophys. Res.* **2001**, *106*, 3591−3601.
(25) Danilin, M. Y.; Shia, R.-L.; Ko, M. K. W.; Weisenstein, D. K.; Sze, N. D.; Lamb, J. J.; Smith, T. W.; Lohn, P. D.; Prather, M. J. *J. Geophys. Res.* **2001**, *106*, 12727−12738.
(26) Hanning-Lee, M. A.; Brady, B. B.; Martin, L. R.; Syage, J. A. *Geophys. Res. Lett.* **1996**, *23*, 1961−1964.
(27) Low, G. K.-C.; McEvoy, S. R.; Matthews, P. W. *Environ. Sci. Technol.* **1991**, *25*, 460−467.
(28) Mijos, K. Cyclic amines. In *Kirk-Othmer Encyclopedia of Chemical Technology*; Wiley: New York, 1978; Vol. 2, pp 295−308.

10.1021/la0487343 CCC: $27.50 © 2004 American Chemical Society
Published on Web 11/24/2004

ment has been addressed.[29,30] Second, nitrogen-containing compounds are common in many environmental systems. For example, over 50% of herbicides and pesticides contain one or more nitrogen atoms in their molecular structures.[31]

In this study, the adsorption of piperidine at the hydrated α-alumina (0001) surface was investigated by using a surface-selective technique, vibrational sum frequency generation (SFG) spectroscopy. This spectroscopic technique has been extensively used within the past decade to study fundamental interfacial phenomena.[32−42] A brief overview of the theory[43,44] is outlined here. Sum frequency generation is a nonlinear optical process, which under the electric-dipole approximation only occurs in a non-centrosymmetric environment, such as at an interface. When a visible photon and an infrared photon interact at the interface, and if an interfacial vibrational mode,ν, is resonant with the frequency of the incident infrared photon, ω_{IR}, an enhanced signal (SFG) with a frequency at the sum of the two incident photon's frequencies will be observed. The SFG intensity, I_{SFG},

$$I_{SFG} \propto |\chi^{(2)}|^2 \propto |\chi^{(2)}_{NR} + \sum_{\nu}\chi^{(2)}_{\nu}|^2 \qquad (1)$$

as shown in eq 1, is proportional to the absolute square of the macroscopic second-order susceptibility, $\chi^{(2)}$, which consists of resonant terms ($\chi^{(2)}_{\nu}$) and a nonresonant term ($\chi^{(2)}_{NR}$). The resonant susceptibility term ($\chi^{(2)}_{\nu}$) dominates the SFG signal in the studies presented here. $\chi^{(2)}_{\nu}$ is shown in eq 2,

$$\chi^{(2)}_{\nu} \propto \frac{A_{\nu}}{\omega_{IR} - \omega_{\nu} + i\Gamma_{\nu}} \qquad (2)$$

where A_{ν} is the amplitude of the transition moment, ω_{ν} is the frequency of the transition moment, and Γ_{ν} describes the line-width of the transition. The amplitude, A_{ν}, is nonzero when the Raman and the infrared transitions are spectroscopically allowed.

The SFG spectrum, which describes the SFG intensity (I_{SFG}) as a function of the incident infrared frequency, can be mathematically fit according to eq 1. When performing the mathematical fit, a constant complex number is used to represent the nonresonant term ($\chi^{(2)}_{NR}$) and the sign of the vibration amplitude (A_{ν}) is used to denote the phase of the resonant photons of the surface vibrational mode, which incorporates orientation and relative vibrational phases. Equation 2 indicates the Lorentzian line shape in the SFG spectrum fitting. The commercially available software, IGOR (version 4.0.5.1), was used in the fitting procedure after adding additional codes to describe the coherent nature of the SFG process as shown in eq 1.

Experimental Section

In the Allen Lab, two types of SFG systems are available. One is a broad bandwidth SFG (BBSFG) system and the other is a scanning SFG system. The BBSFG system was used to investigate the C−H stretching region of surface-adsorbed piperidine. The scanning SFG system was used to investigate the broad hydrogen-bonding region that reveals the O−H stretching resonance at the α-alumina surface. A brief description of both SFG systems is given below.

The BBSFG system consists of two 1 kHz repetition rate regenerative amplifiers (Spectra-Physics Spitfire, femtosecond and picosecond versions), both of which are seeded by a sub-50 fs 792 nm (the wavelength is tuned for system optimization) pulse from a Ti:Sapphire oscillator (Spectra-Physics, Tsunami) and pumped by a 527 nm beam from an all-solid-state Nd:YLF laser (Spectra-Physics, Evolution 30). The two regenerative amplifiers provide 85-fs pulses at 800 nm (22 nm bandwidth) and 2 ps pulses at 800 nm (17 cm^{-1} bandwidth). The femtosecond broad bandwidth pulses are then used to generate broad bandwidth infrared (~600 cm^{-1} bandwidth) light via an optical parametric amplifier (Spectra-Physics, OPA-800CF). To narrow the output bandwidth of the 2 ps 800 nm beam to improve the spectral resolution of the BBSFG system, the compressor of the regenerative amplifier (picosecond version) was modified. A beam mask is positioned in the compressor to partly block the spatially dispersed beam from the compressor grating and only allows a small spectral portion of the dispersed beam to be compressed. This modification spectrally narrows the output beam bandwidth of the formerly 2 ps 800 nm beam from 17 to 5 cm^{-1}. The SFG experiment was then performed in reflection geometry using the narrow bandwidth (5 cm^{-1}) 800 nm beam (~140 μJ) and the broad bandwidth infrared beam (~10 μJ). The broadband infrared and narrowband 800 nm pulses, which were incident on the sample at 66° and 58° from the surface normal, respectively, were overlapped at the sample surface spatially and temporally to produce a vibrationally resonant SFG spectrum. The SFG photons were emitted at 59.3° from the surface normal and were detected using a monochromator−CCD detection system (Acton Research, SpectraPro SP-500 monochromator; Roper Scientific, 1340 pixel × 400 pixel array, LN400EB back-illuminated CCD) with a 1200 g mm^{-1} grating blazed at 750 nm. The polarization combination for these studies was ssp (in the order of SFG, 800 nm, and infrared). The nonresonant SFG spectrum from a GaAs (Lambda Precision Optics, Inc) crystal surface was obtained both with and without a polystyrene film covering the OPA infrared output port. The resulting SFG spectra were used for normalization purpose and as a reference to calibrate the peak positions of the BBSFG spectra. The calibration accuracy is better than 1 cm^{-1}. All of the BBSFG spectra presented in this paper were calibrated and normalized before performing curve-fitting.

When performing BBSFG measurements on the air−solid interface, the α-alumina window was placed on a leveled sample stage and the height of the top alumina surface was adjusted to be at the overlap point of the incident 800 nm and infrared beams. When performing BBSFG measurements on the air−liquid interface, the liquid solution was placed in a Petri dish and the liquid level was adjusted to be at the overlap point of the incident 800 nm and infrared beams. The reflected 800 nm beams from the surfaces (the top surface of the solid, the bottom surface of the solid, the liquid surface or from the dish) were blocked by spatial filters placed after the sample. The scattered 800 nm beam was further filtered out by two SPF-750 filters and two notch filters placed in front of the monochromator entrance slit. The spectra presented here are the average of at least two replicate spectra. The spectra were acquired at the ambient condition of 23 °C and a relative humidity (RH) of 38% and 0%

(29) Bae, H.-S.; Cho, Y.-G.; Oh, S.-E.; Kim, I.-S.; Lee, J. M.; Lee, S.-T. *Chemosphere* **2002**, *48*, 329−334.
(30) Alberici, R. M.; Canela, M. C.; Eberlin, M. N.; Jardim, W. F. *Appl. Catal. B: Environ.* **2001**, *30*, 389−397.
(31) Packer, K. *Nanogen Index: A Dictionary of Pesticides and Chemical Pollutants*; Nanogens International: Freedom, CA, 1975.
(32) Zhu, X. D.; Suhr, H.; Shen, Y. R. *Phys. Rev. B: Condens. Matter* **1987**, *35*, 3047−3050.
(33) Miranda, P. B.; Shen, Y. R. *J. Phys. Chem. B* **1999**, *103*, 3292−3307.
(34) Cremer, P. S.; Su, X.; Somorjai, G. A.; Shen, Y. R. *J. Mol. Catal. A: Chem.* **1998**, *131*, 225−241.
(35) Richmond, G. L. *Chem. Rev.* **2002**, *102*, 2693−2724.
(36) Allen, H. C.; Raymond, E. A.; Richmond, G. L. *Curr. Opin. Colloid Interface Sci.* **2000**, *5*, 74−80.
(37) Shultz, M. J.; Baldelli, S.; Schnitzer, C.; Simonelle, D. *J. Phys. Chem. B* **2002**, *106*, 5313−5324.
(38) Wang, C.-Y.; Groenzin, H.; Shultz, M. J. *J. Phys. Chem. B* **2004**, *108*, 265−272.
(39) Wang, J.; Clarke, M. L.; Chen, Z. *Anal. Chem.* **2004**, *76*, 2159−2167.
(40) Briggman, K. A.; Stephenson, J. C.; Wallace, W. E.; Richter, L. J. *J. Phys. Chem. B* **2001**, *105*, 2785−2791.
(41) Ma, G.; Allen, H. C. *J. Phys. Chem. B* **2003**, *107*, 6343−6349.
(42) Liu, D.; Ma, G.; Levering, L. M.; Allen, H. C. *J. Phys. Chem. B* **2004**, *108*, 2252−2260.
(43) Shen, Y. R. *The Principles of Nonlinear Optics*, 1st ed.; John Wiley and Sons: New York, 1984.
(44) Zhuang, X.; Miranda, P. B.; Kim, D.; Shen, Y. R. *Phys. Rev. B* **1999**, *59*, 12632−12640.

with a 5 min CCD acquisition time. The BBSFG investigation under 38% RH was performed by placing the alumina into a sealed bottle with saturated piperidine vapor for 5 min (vapor pressure of piperidine = 28.3 Torr at 25 °C[45]) and then placing the alumina crystal back onto the sample stage to investigate the air−solid interface. The BBSFG investigation under 0% RH was performed with a home-built SFG cell. The cell was equipped with a BaF_2 window as the optical input port and a BK7 window as the optical output port. There is one gas inlet at the bottom of the cell and one gas outlet at the top of the cell. The freshly annealed alumina single crystal was kept under ambient conditions (47% RH) for more than 30 min to allow the surface to become hydrated (i.e., hydroxylated), and then the crystal was placed into the cell. The cell was purged with H_2O-free air (generated by a Balston FTIR purge gas generator, model 75−62) for 1 h to remove physisorbed water from the alumina surface and afterward continuous purging was maintained throughout the experiment. A small amount (0.25 mL) of piperidine liquid was introduced into the inlet gas tubing, and the purging gas carried piperidine vapor into the cell to interact with the alumina surface. After 1 h of purging, the BBSFG spectrum from the alumina surface was recorded in situ.

The scanning SFG system was used to acquire the O−H stretching region of the spectra from the surface of the alumina. This system utilizes a visible beam at 532 nm and an infrared beam tunable from 2500 to 4000 cm^{-1} with a bandwidth of ~4−8 cm^{-1} depending on the spectral region. The 532 nm beam is generated by doubling the frequency (second harmonic) of the 1064 nm pump source from an EKSPLA PL 2143A/SS Nd:YAG laser (29 ps pulse duration and 10 Hz repetition rate). The infrared beam is generated from a KTP−KTA-based optical parametric generator/amplifier (OPG/OPA) system (LaserVision). The input 532 nm intensity is focused using a plano-convex lens (CVI Laser, 500 mm focal length) and is placed ~490 mm before the sample surface to provide an ~1 mm beam diameter and 400 μJ per pulse of 532 nm light on the sample surface. The infrared is focused at the sample surface using a BaF_2 lens (200 mm focal length), where it has <0.5 mm beam diameter, and is ~400 μJ per pulse. The input angles are ~45° and ~53° from the surface normal for the 532 nm and infrared beams, respectively. The detection angle is set to 45.6° from the surface normal for sum frequency detection. Several spatial, Schott glass, and notch filters are used to block the 532 nm beam from entering the detection system. A 512 pixel × 512 pixel array, 12.3 mm × 12.3 mm active area, 24 μm square pixel size, back illuminated CCD (DV412, Andor Technology) is used to detect the sum frequency signal. The CCD is thermo-electrically cooled and the CCD temperature was set at −45 °C during the experiments. A home-written program in Labview and C+ languages was used for data acquisition. The scanning SFG spectra presented in this paper were acquired using a 10 s exposure time for each data point, and spectra were acquired in 20 min (from 2700 to 4000 cm^{-1}). The spectra presented here are the average of at least two replicate spectra. The polarization combination used for the scanning SFG experiments presented here are s, s, and p for the SFG, 532 nm, and infrared beams, respectively. The nonresonant response from the GaAs surface was used for normalization. The scanning SFG spectra were acquired at the ambient condition of 21 °C and 35% RH.

The Raman experimental setup consists of a 532 nm CW laser (Spectra-Physics, Millennia II), a 5 mm focusing Raman Probe (InPhotonics, RP 532-05-15-FC.), a 500 mm monochromator (Acton Research, SpectraPro SP-500) using a 600 g mm^{-1} grating and a back-illuminated CCD (Roper Scientific, LN400EB, 1340 pixel × 400 pixel array and deep depletion). Raman spectra were collected using a fiber optic, which was coupled to the entrance slit of the monochromator through a fiber optic imaging coupler (Acton Research, FC-446-030). SpectraSense software (Acton Research version 4.1.9) was used for data collection and display. The power of the 532 nm beam for sample illumination was 90 mW. Before data collection, the Raman system was calibrated by using the 435.83 nm line of a fluorescence lamp and was verified by comparison to the Raman spectrum of naphthalene. The Raman spectral resolution and acquisition temperature were 0.8 cm^{-1} and ~23 °C. The sample was placed in a glass vial. The sample glass vial was placed in a home-built sample holder, which holds both the sample vial and the Raman probe. The alignment of the Raman probe in the sample holder can affect the detected Raman intensity to some extent. The intensity variation can be normalized by taking a Raman spectrum of a reference sample (i.e., neat piperidine in this study) when comparison of the Raman intensity between different samples is necessary.

A Thermo Nicolet FTIR spectrometer (Avatar 370, Thermo Electron Corporation) was employed in the FTIR spectroscopy experiments. The spectrometer is equipped with a DTGS KBr detector and purged with hydrocarbon-H_2O-CO_2-free air. Spectra were collected with a spectral resolution of 4 cm^{-1} and 128 scans at a temperature of ~ 24 °C. A demountable IR cell equipped with a pair of CaF_2 windows was utilized. The second derivative method was used to obtain the positions of the overlapped peaks in the FTIR spectrum as a resolution enhancement technique.

The XPS measurements were performed with a Kratos Axis Ultra photoelectron spectrometer. Experiments were conducted at room temperature with a base pressure in the 4.4×10^{-10} Torr range. The monochromatic Al Kα X-ray source was operated at 130 W (1.3 kV, 10 mA). Survey spectra were acquired at a pass energy of 80 eV with 100 ms dwell time to determine the surface contamination.

The pH measurements of aqueous solutions were performed with a pH meter from Oakton Instruments (pH Testr 3+ Double Junction) at the ambient temperature of 22 °C. The pH meter was calibrated with Fisher Scientific buffer solutions. Values are averages of three readings.

Surface tensions were measured at the ambient temperature of 22 °C using a surface tensiometer (DeltaPi, Kibron Inc., Finland), which employs the Wilhelmy method. Values are averages of five readings.

The α-Al_2O_3 single-crystal (c-cut, (0001) plane) parallel windows (1 in. in diameter and 1/4 in. thick) were purchased from Marketech International (Port Townsend, WA) with a purity of 99.995%. The crystal was highly polished with a surface quality of 20-10 (it has been found in this study that crystals without a highly polished surface can more efficiently generate white light by high-intensity 532 nm input). The crystal was investigated by XPS after being received from the supplier to make certain that there was no inorganic contamination (especially silica) at the alumina surface. The XPS spectrum is shown in Figure 1A. Before the SFG experiments, the alumina crystal was annealed in a muffle oven (Fisher Scientific, Isotemp Muffle Furnace) at 900 °C for more than 12 h in order to remove possible organic contamination. After the crystal was cooled to room temperature, the crystal was kept under ambient conditions for more than 30 min to allow its equilibrium with the water vapor in the air. Then, the SFG experiments were performed on the alumina surface before and after the piperidine adsorption.

It has been reported that using laboratory glassware to handle alumina may cause silica contamination at the alumina surface.[46−49] This has been observed in this study when soaking alumina in water in glass containers, as shown in the XPS spectrum in Figure 1B. The data shown in this study were obtained from the silica-free alumina surface. It has been found in this study that the silica contamination can affect the SFG spectrum of the alumina surface, especially in the O−H stretch region, i.e., causing changes in the aluminol OH peak intensity.

Analytical grade piperidine (99%) obtained from Aldrich and Nanopure water of 18.2 MΩ·cm resistivity were used to make aqueous piperidine solutions. ACS grade HCl (37%) was purchased from Fisher Scientific. The commercial chemicals were used as received. Piperidium chloride was synthesized by reacting piperidine with HCl solution and the needle-like white polycrystalline product was air-dried. Glassware was thoroughly cleaned with an ammonium persulfate sulfuric acid solution.

(45) Das, A.; Frenkel, M.; Gadalla, N. A. M.; Kudchadker, S.; Marsh, K. N.; Rodgers, A. S.; Wilhoit, R. C. *J. Phys. Chem. Ref. Data* **1993**, *22*, 659−782.

(46) Furlong, D. N.; Freeman, P. A.; Lau, A. C. M. *J. Colloid Interface Sci.* **1981**, *80*, 20−31.

(47) Franks, G. V.; Meagher, L. *Colloids Surf., A* **2003**, 214, 99−110.

(48) Stack, A. G.; Higgins, S. R.; Eggleston, C. M. *Geochim. Cosmochim. Acta* **2003**, *67*, 321−322.

(49) Kosmulski, M. *Geochim. Cosmochim. Acta* **2003**, *67*, 319−320.

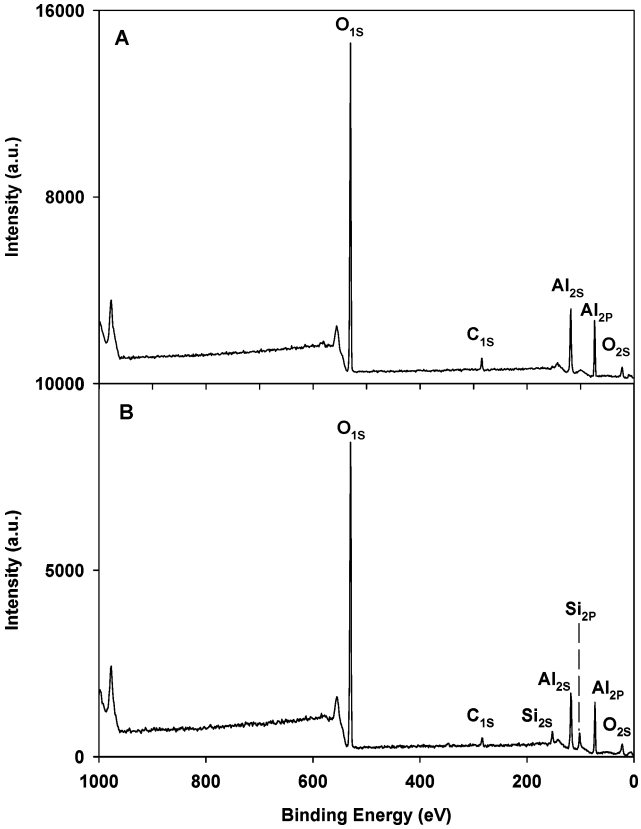

Figure 1. Characteristic XPS survey of the α-alumina (0001) surface. (A) Clean alumina surface and (B) silica-contaminated alumina surface.

Since an SFG-active vibrational mode must be both IR-active and Raman-active, an IR spectrum and a Raman spectrum of the chemicals of interest were obtained and analyzed before performing the SFG spectrum curve-fit. By performing curve-fits on the IR and Raman spectra, the number of peaks, peak position, and bandwidth of both Raman and IR active modes can be obtained. These peak parameters are used as references when setting the initial guess and the confinement parameters in the SFG curve-fitting process, as well as determining the possible numbers of the peaks that can exist in the SFG spectrum.

Results and Discussion

To fully understand piperidine adsorption on the alumina surface, prior elucidation of the hydroxylated alumina surface is crucial. Figure 2 shows the air−solid interfacial scanning SFG spectrum obtained from the alumina (0001) surface under ambient conditions with 35% RH. The scanning SFG spectrum reveals a broad spectral profile and a sharp free OH peak (dangling OH) within the O−H stretching region of 3000−3800 cm^{-1}. In the free OH region, both the free OH stretching of adsorbed water molecules and the free aluminol OH stretching can contribute to the SFG response. The free OH stretch of the dangling water OH at the air−water interface is at ∼3700 cm^{-1}.[42,50−52] The aluminol OH stretch with the oxygen coordinated by three aluminum atoms has been previously observed at ∼3710 cm^{-1} via infrared spectroscopy.[53−56] The broad band observed from 3000 to

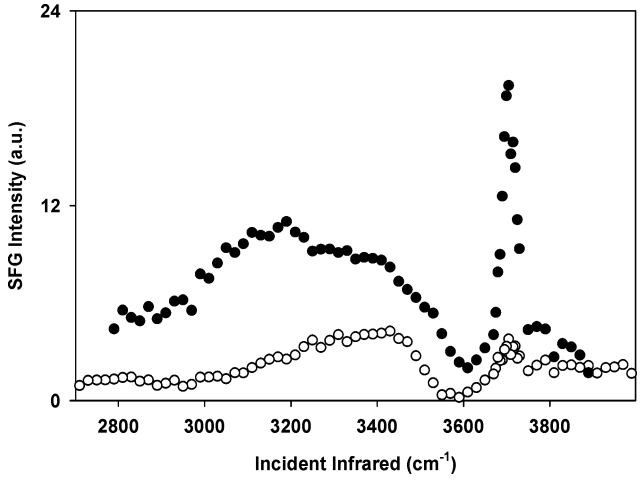

Figure 2. Scanning SFG spectra of the air−solid interface of hydrated α-alumina (0001) surface (open circles) and the air−liquid interface of neat water (solid circles).

3600 cm^{-1} is assigned to molecularly adsorbed water and hydrogen-bonded surface hydroxyl (AlO−H- - -). This is consistent with previous assignments for alumina surface hydroxyls[7,53−57] and water at the air−water interface.[42,50−52] The difference between the air−alumina spectrum and the air−water spectrum in the broad O−H stretching region of 3000−3600 cm^{-1} as shown in Figure 2 indicates that the hydrogen-bonding network at the alumina surface is different from that of the air−water interface. It is also noted that there is a baseline increase in the SFG spectrum of the air−alumina interface from 3700 to 4000 cm^{-1}. This baseline increase is consistent with previous FTIR studies of the alumina (0001) surface.[57]

The α-Al_2O_3 single crystal surface has been extensively studied in recent years.[6−8,11,12,57,58] A brief discussion is therefore presented here because of its relevance to this research. Previous studies on single-crystal α-Al_2O_3 surfaces can be classified into two types: ultrahigh vacuum (UHV), and in the presence of water vapor (typically under ambient conditions). The surface structures of the alumina (0001) surface under the two conditions are completely different. Under UHV conditions, theoretical prediction[59] and experimental investigation[10] have revealed that the (0001) surface is relaxed and terminated with an aluminum layer. The relaxation is believed to consist of a large, nearly bond-length-conserving displacement of the surface atoms from their bulk positions.[59] This eventually results in an energetically favorable Al-terminated layer. Compared with the relatively simple surface structure under UHV conditions, the structure of the alumina (0001) surface under ambient conditions is far more complicated due to exposure to ambient water vapor. The interaction of alumina at the (0001) surface with gas-phase water results in significant modifications of the alumina surface structure. Recent ab initio studies have indicated that H_2O can be dissociatively adsorbed on the alumina surface, resulting in an O-terminated outermost layer.[7] The H_2O dissociation produces two distinct types of surface

(50) Allen, H. C.; Raymond, E. A.; Richmond, G. L. *J. Phys. Chem.* **2001**, *105*, 1649−1655.
(51) Du, Q.; Superfine, R.; Freysz, E.; Shen, Y. R. *Phys. Rev. Lett.* **1993**, *70*, 2313−2316.
(52) Schnitzer, C.; Baldelli, S.; Campbell, D. J.; Shultz, M. J. *J. Phys. Chem. A* **1999**, *103*, 6383−6386.
(53) Knozinger, H.; Ratnasamy, P. *Catal. Rev. − Sci. Eng.* **1978**, *17*, 31−70.
(54) Ballinger, T. H.; Yates, J. T., Jr. *Langmuir* **1991**, *7*, 3041−3045.
(55) Mawhinney, D. B.; Rossin, J. A.; Gerhart, K.; Yates, J. T., Jr. *Langmuir* **2000**, *16*, 2237−2241.
(56) Ivey, M. M.; Layman, K. A.; Avoyan, A.; Allen, H. C.; Hemminger, J. C. *J. Phys. Chem. B* **2003**, *107*, 6391−6400.
(57) Al-Abadleh, H. A.; Grassian, V. H. *Langmuir* **2003**, *19*, 341−347.
(58) Liu, P.; Kendelewicz, T.; Brown, G. E., Jr.; Nelson, E. J.; Chambers, S. A. *Surf. Sci.* **1998**, *417*, 53−65.
(59) Godin, T. J.; LaFemina, J. P. *Phys. Rev. B* **1994**, *49*, 7691−7696.

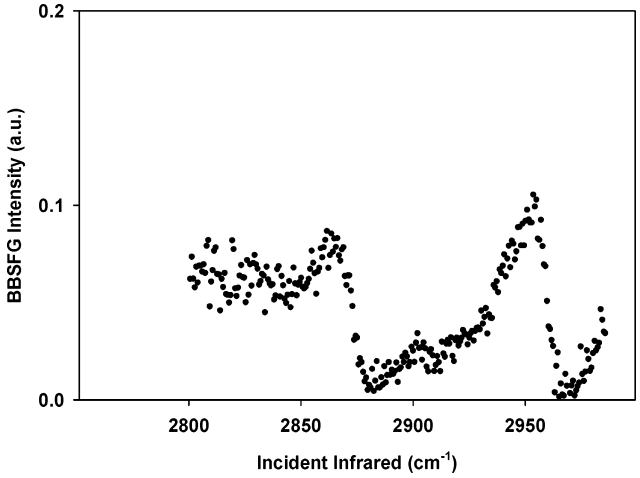

Figure 3. BBSFG spectrum of the air−solid interface of hydrated α-alumina (0001) surface after piperidine adsorption. The alumina crystal was exposed to piperidine vapor for 5 min.

hydroxyl groups: $O_{ads}H$ and O_sH. The $O_{ads}H$ originates from surface water molecules, and the O_sH originates from the surface oxygen of the alumina. The two types of surface hydroxyl groups have different infrared frequencies found at ~3780 cm^{-1} for $O_{ads}H$ and 3450 cm^{-1} for O_sH due to the differing Al−O coordination. The 3780 cm^{-1} value is in good agreement with the assignment for the terminal OH on a 4-fold-coordinated Al. The O_sH is typically assigned to a broad peak which overlaps with the molecularly adsorbed H_2O bands ranging from 3400 to 3600 cm^{-1}. The broad surface hydroxyl O_sH feature is then complicated by the hydrogen-bonding network resonances. This interpretation is consistent with studies on the desorption of molecular H_2O from the hydroxylated single-crystal α-Al_2O_3 (0001) surface using laser-induced thermal desorption (LITD) and temperature-programmed desorption (TPD) techniques.[12] The large temperature range for H_2O desorption observed suggested a variety of hydroxyl surface sites with different binding energies. The existence of molecularly adsorbed H_2O in addition to the surface hydroxyl at the α-alumina (0001) surface was also confirmed in a recent study of crystal truncation rod X-ray diffraction performed under ambient conditions.[6] Their result suggested that there was a physisorbed (hydrogen-bonded) water layer on top of the surface hydroxyl layer. In an FTIR study performed on the (0001) α-alumina surface under different humidity conditions, it was found that at humidities higher than 10% molecularly adsorbed H_2O exists at the alumina surface, which can form a structured overlayer when the humidity is between 10% and 70%.[57] Additionally, this study revealed that a quasi-liquid layer was formed when humidity was higher than 70%.

On the basis of the SFG results, as shown in Figure 2, in addition to previous studies by others,[6,7,57] the hydrated α-Al_2O_3 (0001) surface at 35% RH can be described as a hydrogen-bonding network formed by molecularly adsorbed water in addition to surface hydroxyl groups hydrogen-bonded to the adsorbed water. The piperidine vapor used in the adsorption experiments is expected to interact with this hydrogen-bonded water layer and/or directly with the surface hydroxyl groups of alumina. The studies are presented below.

Figure 3 shows the BBSFG spectrum of the air−Al_2O_3 interface after the Al_2O_3 was exposed to piperidine vapor for 5 min. At least two SFG peaks are observed in the C−H stretching region after alumina was exposed to the piperidine vapor. Clearly, piperidine molecules are adsorbed onto the Al_2O_3 surface, as indicated by the observed peak frequencies that correspond to piperidine vibrational frequencies. (Spectral fits and assignments are presented in the following sections.)

The observed peak frequencies shown in Figure 3 are slightly different from previously published piperidine frequencies.[60−63] A frequency shift of the CH_2 peaks is what one would expect to observe if piperidine is interacting with the alumina surface hydroxyl groups and/or the surface-adsorbed water. The interaction between piperidine and the alumina surface can be elucidated by comparison to spectroscopic signature frequencies of other carefully chosen systems, and therefore, additional studies were conducted.

Three adsorption mechanism scenarios are shown in Figure 4 based on the hydrated surface structure of α-alumina as discussed above. Scenario I is a hydrogen-bonding model in which piperidine is adsorbed to either the water layer or the surface hydroxyl groups through formation of a hydrogen bond. Recent ab initio calculations indicated that amines can only act as hydrogen-bonding acceptors by donating the N electron lone pair when interacting with H_2O.[64] Therefore, in this model scenario, the amine group of piperidine only acts as a hydrogen-bonding acceptor. The methylene groups are not expected to strongly interact with the surface.

Scenario II is a protonation model in which piperidine is protonated by a surface water molecule or surface hydroxyl. Recall that piperidine is a strong organic base with a pK_a of 11.07;[65,66] therefore, it is reasonable to expect water to protonate piperidine. On the other hand, the reported isoelectric point (IEP) of α-Al_2O_3 is 9,[47] suggesting that the alumina surface hydroxyl group is an unlikely protonating agent. However, the IEP literature value was obtained from measurements on α-Al_2O_3 powders. More recent studies have shown that, at the single-crystal α-Al_2O_3 (0001) surface, the IEP value is ~5,[47,67,68] implying that the surface hydroxyl groups of the single-crystal α-Al_2O_3 (0001) surface can be more acidic than H_2O. From Scenario II, two protonation options are included and both are possible candidates.

Scenario III is a quasi-liquid layer model in which piperidine forms a liquidlike layer at the alumina surface. In this model, the piperidine predominately interacts with other piperidine molecules. Previous studies indicated that piperidine has a weak tendency to form a piperidine dimer through an intermolecular hydrogen-bonding interaction.[69] Though the dimerization tendency is weak, the dimer species was included to provide a complete picture of the quasi-liquid layer model. Other possible scenarios might include the formation of an Al−N bond; however, this is considered an unlikely model candidate in this study since there are no unoccupied Al coordination sites available.

(60) Sanchez, L. A.; Birke, R. L.; Lombardi, J. R. *J. Phys. Chem.* **1984**, *88*, 1762−1766.
(61) Titova, T. V.; Anisimova, O. S.; Pentin, Y. A. *Opt. Spectrosc. (Engl. Transl.)* **1967**, *32*, 495−497.
(62) Vedal, D.; Ellestad, O. H.; Klaboe, P. *Spectrochim. Acta* **1976**, *32A*, 877−890.
(63) Krueger, P. J.; Jan, J. *Can. J. Chem.* **1970**, *40*, 3236−3248.
(64) Rablen, P. R.; Lockman, J. W.; Jorgensen, W. L. *J. Phys. Chem. A* **1998**, *102*, 3782−3797.
(65) Palm, V. A. *Tables of rate and equilibrium constants of heterolytic organic reactions*; Academy of Sciences of the USSR: Moscow, 1976; Vol. 2(1).
(66) Kallies, B.; Mitzner, R. *J. Phys. Chem. B* **1997**, *101*, 2959−2967.
(67) Kershner, R. J.; Bullard, J. W.; Cima, M. J. *Langmuir* **2004**, *20*, 4101−4108.
(68) Larson, I.; Drummond, C. J.; Chan, D. Y. C.; Grieser, F. *Langmuir* **1997**, *13*, 2109−2112.
(69) Janossy, A. G. S.; Demeter, S. *Spectrosc. Lett.* **1975**, *8*, 805−810.

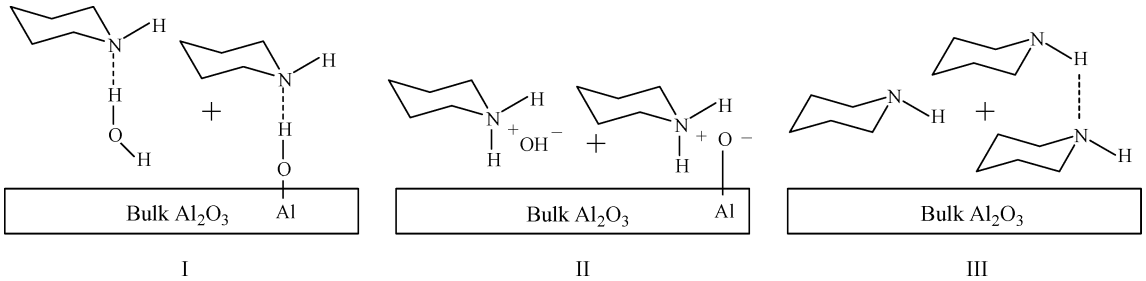

Figure 4. Schematic of the three possible adsorption scenarios of piperidine at the hydrated α-alumina (0001) surface: (I) hydrogen-bonding, (II) protonation, and (III) liquidlike.

To evaluate the viability of the three scenarios shown in Figure 4, we have used one of the piperidine vibrational modes in the C−H stretching region as a spectroscopic probe. (The N−H stretch vibrations are not used as a probe since these peaks overlap with the O−H stretch region. In addition, the N−H of piperidine also takes part in hydrogen bonding which broadens the peaks.) Recall that the vibrational frequency provides information on the strength of the chemical bond which is influenced by the chemical environment. If we can identify frequency shifts of the piperidine C−H stretching vibrations upon formation of hydrogen bonds or protonation, it is possible to distinguish between hydrogen-bonded piperidine, protonated piperidine, and liquidlike piperidine. The following three spectra were used to establish a reference system: the BBSFG spectra as shown in Figure 5 of the air−neat piperidine interface (Figure 5A), the air−aqueous piperidine interface (Figure 5B), and the air−aqueous piperidium chloride interface (Figure 5C). The three spectra establish reference vibrational frequencies for liquidlike piperidine, H-bonded piperidine by surface OH and/or surface water, and protonated piperidine by surface OH and/or surface water. Clearly, these spectra are quite different from each other. As expected, spectral features of piperidine are sensitive to chemical environment.

To compare the CH_2 vibrational frequencies of piperidine in the reference spectra shown in Figure 5A−C to that of the SFG spectrum of piperidine adsorbed onto the alumina surface shown in Figure 3, curving-fitting was performed in order to obtain accurate peak positions free of overlapping neighbor peaks. The SFG peak fitting is completed utilizing fitting parameters from Raman and IR spectra. The Raman and IR spectra of neat piperidine and their fits are shown in Figure 6. The second-derivative method provided the initial guesses for peak positions and number of peaks in the Raman and FTIR fittings of neat piperidine. The seven peaks used to fit both the Raman and IR spectra and the fitted peak positions, as well as the peak positions obtained by the second-derivative technique, are listed in Tables 1 and 2. The fitted IR peaks and the second-derivative peaks of neat piperidine are consistent with each other. The spectral assignments for the neat piperidine peaks are based on previous studies.[60−63]

A piperidine molecule has two α-methylene groups, two β-methylene groups, and one γ-methylene group. Piperidine can also exist as two conformers, equatorial and axial.[70] The Raman 2854 cm^{-1} peak (2851 cm^{-1} for IR) and 2933 cm^{-1} peak (2932 cm^{-1} for IR) are assigned to the CH_2 symmetric stretch (CH_2-SS) and asymmetric stretch (CH_2-AS) of the γ-methylene and β-methylene groups. The four Raman peaks at 2732 (2730 for IR), 2803 (2799 for IR), 2893 (2897 for IR) and 2916 (2918 for IR) cm^{-1} are assigned to the α-methylene groups in-phase and out-of-phase couplings. Previous studies showed that when one α-methylene group is deuterated, the coupling effect will disappear and the two peaks at 2732 and 2803 cm^{-1} will become one peak at around 2760 cm^{-1}.[63] The Raman 2947 cm^{-1} peak (2943 cm^{-1} for IR) observed here was not

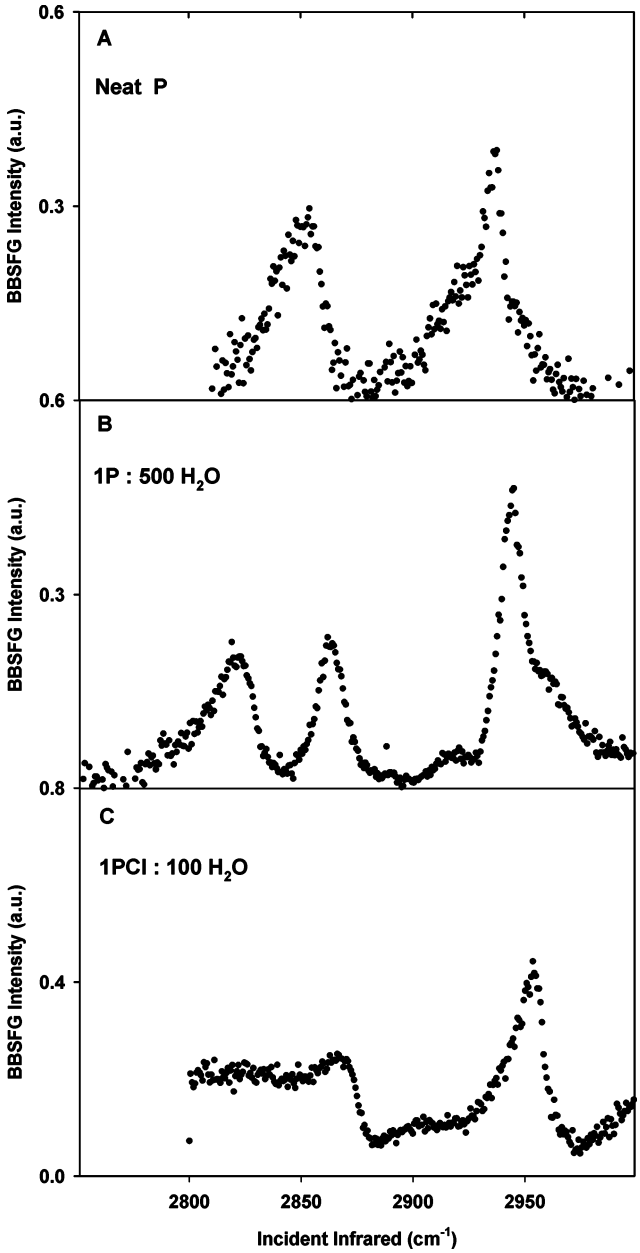

Figure 5. BBSFG spectra of (A) the air−neat piperidine interface, (B) the air−aqueous piperidine interface with a 1:500 mole ratio between piperidine and H_2O, and (C) the air−aqueous piperidium chloride interface with a 1:100 mole ratio between piperidium chloride and H_2O. P, piperidine; PCl, piperidium chloride.

(70) Scott, D. W. *J. Chem. Thermodyn.* **1971**, *3*, 649−656.

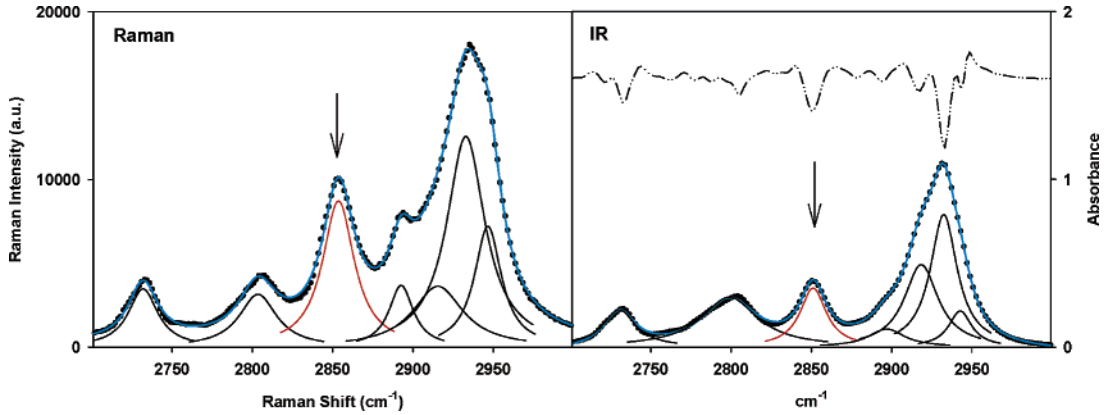

Figure 6. Raman and FTIR spectra of neat piperidine: solid circles, experimental; solid line, Lorentzian fit; blue line, overall fit; dot−dash, the second derivative spectrum; red line, probe peak.

Table 1. Fitting Results and Assignments of the Raman Spectra of Neat Piperidine, Aqueous Piperidine Solutions, and Aqueous Piperidium Chloride Solutions[a]

	CH_2-SS (cm^{-1})			CH_2-AS (cm^{-1})						
neat piperidine	2732	2803	2854	2893		2916	2933	2947		
piperidine: H_2O (1:10)	2732	2802	2853	2891	2903		2931	2944	2957	
piperidine:H_2O (1:100)	2752		2862		2911			2945	2960	
piperidium chloride:H_2O (1:10)	2775		2874		2905	2926	2935	2961	2973	3002
piperidium chloride:H_2O (1:100)	2777		2875		2907	2927	2936	2964	2976	3005

[a] (1:10) and (1:100) are mole ratios.

Table 2. Fitting and Second-Derivative Results and Assignments of the FTIR Spectra of Neat Piperidine, Aqueous Piperidine Solutions, and Aqueous Piperidium Chloride Solutions[a]

	CH_2-SS (cm^{-1})			CH_2-AS (cm^{-1})					
neat piperidine	2730	2799	2851	2897		2918	2932	2943	
neat piperidine (2^{nd})	2733	2805	2851	2894		2917	2933	2943	
piperidine:H_2O (1:10) (2^{nd})	2740	2805	2858	2887	2907		2935	2943	2953
piperidium chloride:H_2O (1:10) (2^{nd})	2774		2873		2902	2920	2937	2959	2968

[a] (2^{nd}) means second derivative; (1:10) is the mole ratio.

reported in previous studies. As shown in Figure 6, this peak is clearly resolved by the second-derivative technique and is tentatively assigned to the CH_2-AS of the equatorial conformer.[63] The CH_2-SS peaks of the two conformers cannot be resolved in this study, and therefore, the 2854 cm^{-1} peak is assigned to two conformers since both of the conformers have been shown to exist in liquid.[63]

The neat piperidine fitting parameters as discussed above were used as references for fitting the Raman spectra of the aqueous piperidine and aqueous piperidium chloride solutions. Due to the strong H_2O absorption interferences, the peak positions in the IR spectra of the aqueous piperidine and aqueous piperidium chloride solutions were obtained only from the second derivative spectra.

The Raman spectra of the aqueous systems are shown in Figure 7A−D, and the peak frequencies from the Raman fits and the FTIR second derivative spectra are listed in Tables 1 and 2.

As revealed in Figure 7A−D, protonation and the presence of water can dramatically change the piperidine spectrum. For example, the CH_2-SS (2803 cm^{-1}) peak intensity diminishes at the higher H_2O concentration (mole ratio = 1:100) (Figure 7B), and upon protonation (Figure 7C−D). The peak frequency of the CH_2-SS (2854 cm^{-1}) is shifted to higher frequency (blue-shifted) due to the addition of water and protonation, as revealed by the dashed line in Figure 7. Protonation causes the greatest blue-shift. The peaks at 2957 and 2960 cm^{-1} (Figure 7A−B) in the aqueous piperidine solutions and the peaks at 2973 and 2976 cm^{-1} (Figure 7C−D) in the aqueous piperidium solutions are newly observed peaks compared to the neat piperidine spectrum and are assigned to the CH_2-AS of hydrogen-bonded piperidine and the CH_2-AS of protonated piperidine.

On the basis of the Raman and FTIR results, the CH_2-SS peak at ~2854 cm^{-1}, as denoted by the red lines in Figure 6, was selected as the spectroscopic probe in this study since it resides in a relatively clean spectral region and its frequency is sensitive to the chemical environment variations such as the addition of water and protonation.

Using the parameters obtained from the Raman and IR fits, the three reference spectra in Figure 5A−C were fitted. These fits are shown in Figure 8A−C. The fitted peak frequencies are listed in Table 3. At the air−neat piperidine interface (Figure 8A), where piperidine does not form a hydrogen bond with H_2O, the CH_2-SS probe peak lies in the low-frequency region of the observed shifts, at 2854 cm^{-1}. At the air−aqueous piperidine interface (Figure 8B), where piperidine interacts with H_2O and forms a hydrogen bond by donating the nitrogen lone electron pair, the CH_2-SS is blue-shifted to ~2862 cm^{-1}. The blue-shift magnitude depends on the amount of water in the piperidine, as shown in Table 3. The higher the H_2O concentration, the larger the blue-shift. At the air−aqueous piperidium chloride interface (Figure 8C), the CH_2-SS peak frequency is further blue-shifted to 2874 cm^{-1}. Considering that piperidine can be protonated by H_2O, as indicated by the basic pH values of aqueous piperidine solutions in Table 3, the BBSFG spectrum of the air−aqueous piperidine interface (Figure 8B) is expected to have spectral contributions from both hydro-

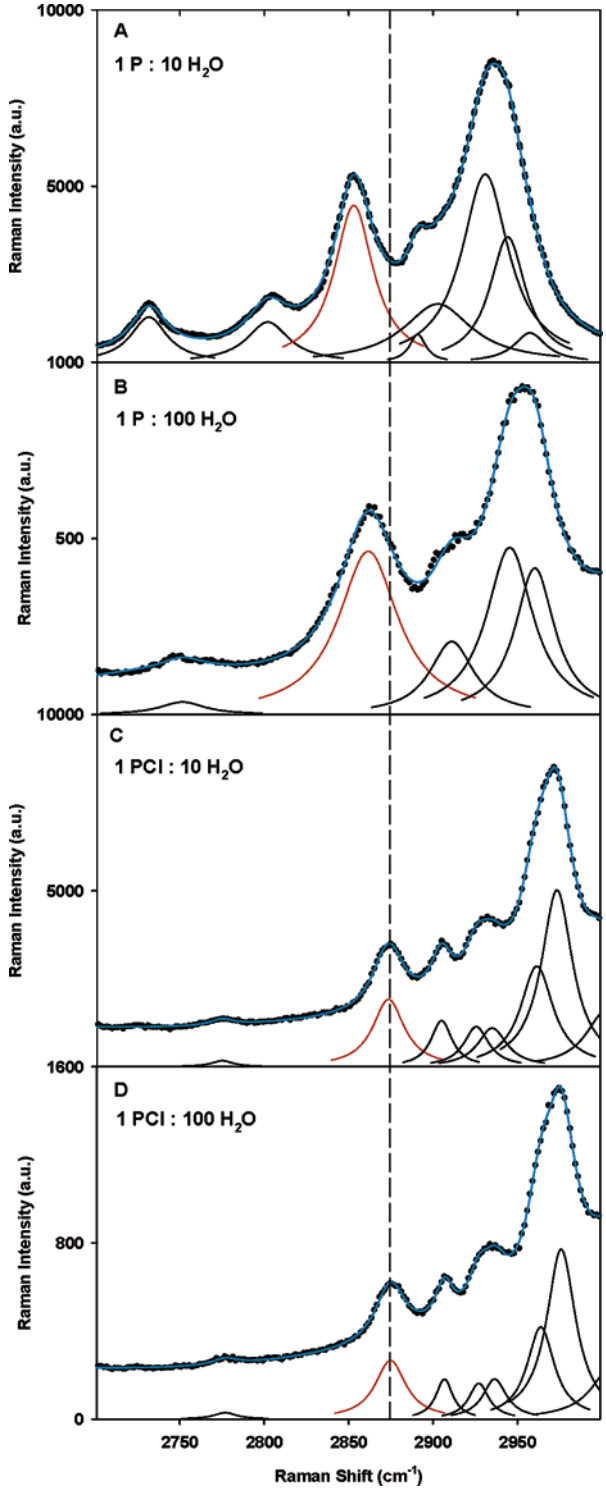

Figure 7. Raman spectra of (A) aqueous piperidine with a 1:10 mole ratio between piperidine and H_2O, (B) aqueous piperidine with a 1:100 mole ratio between piperidine and H_2O, (C) aqueous piperidium chloride with a 1:10 mole ratio between piperidium chloride and H_2O, and (D) aqueous piperidium chloride with a 1:100 mole ratio between piperidium chloride and H_2O: solid circles, experimental; solid line, Lorentzian fit; blue line, overall fit; red line, probe peak; P, piperidine; PCl, piperidium chloride. The dashed line shows the variation of the probe peak positions in different solutions.

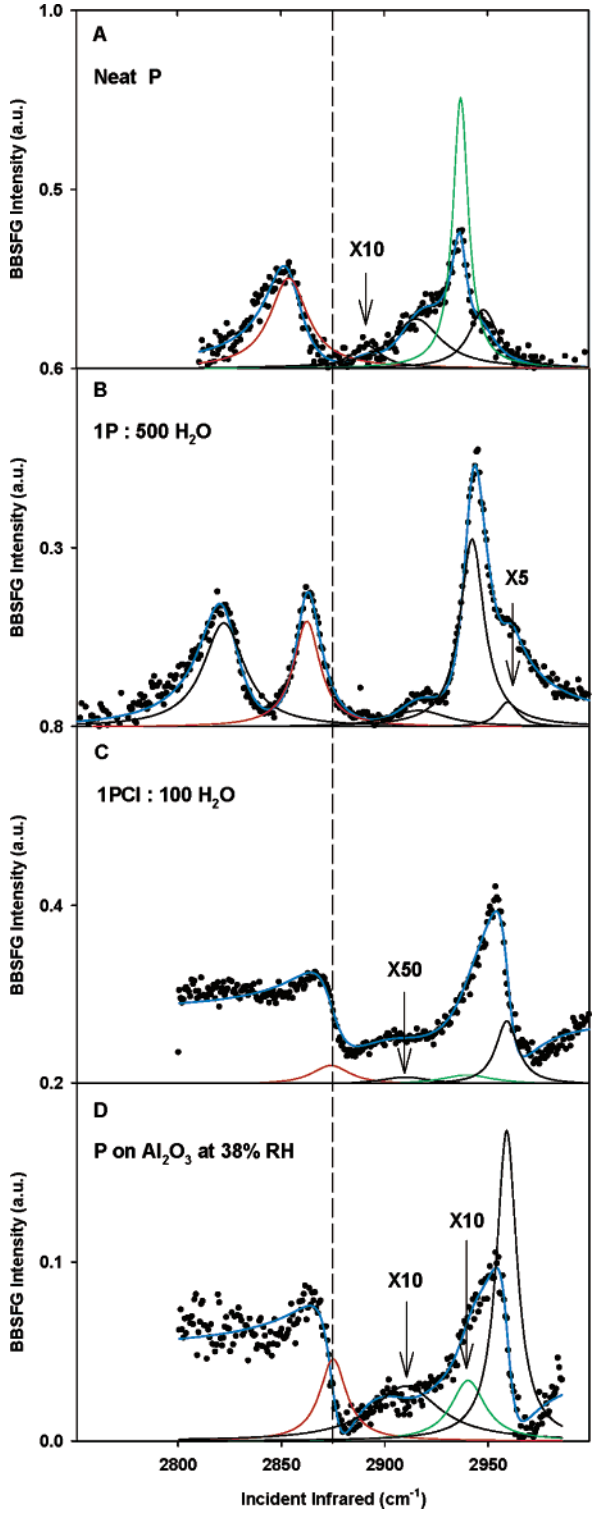

Figure 8. Spectral comparison of the BBSFG spectra of (A) the air−neat piperidine interface, (B) the air−aqueous piperidine interface with a 1:500 mole ratio between piperidine and H_2O, (C) the air−aqueous piperidium chloride interface with a 1:100 mole ratio between piperidium chloride and H_2O, and (D) the air−alumina interface after piperidine adsorption under 38% RH: solid circles, experimental; solid line, Lorentzian fit; blue line, overall fit; red line, probe peak; green line, peak with negative phase in the SFG fitting; P, piperidine; PCl, piperidium chloride. The dashed line shows the variation of the probe peak positions at different surfaces; ×5, ×10, and ×50 denote peak magnification.

gen-bonded piperidine and protonated piperidine. However, the presence of the CH_2-SS at ~2820 cm^{-1} in the BBSFG spectrum of the air−aqueous piperidine interface (Figure 8B), which is not present in the BBSFG spectrum of the air−aqueous piperidium chloride interface (Figure 8C), indicates the dominating presence of hydrogen-bonded piperidine (lack of protonated piperidine) at the

Table 3. Fitting Results and Assignments of the BBSFG Spectra from the Air−Liquid Interfaces of Neat Piperidine, Aqueous Piperidine Solutions, and Aqueous Piperidium Chloride Solutions and the Air−Alumina Interface after the Piperidine Adsorption under 38% RH and 0% RH[a]

	CH_2-SS (cm^{-1})		CH_2-AS (cm^{-1})			
neat piperidine		2854	2891	2915	2937	2948
piperidine:H_2O (1:10) (pH = 12.86)	2820	2860		2919	2941	2953
piperidine:H_2O (1:100) (pH = 12.31)	2821	2861		2913	2942	2955
piperidine:H_2O (1:500) (pH = 11.87)	2822	2862		2916	2942	2959
piperidine:H_2O (1:1000) (pH = 11.62)	2823	2862		2922	2942	2964
piperidium chloride:H_2O (1:100) (pH = 2.93)		2874		2910	2940	2959
Al_2O_3−piperidine (38% RH)		2875		2910	2940	2959
Al_2O_3−piperidine (0% RH)		2874		2907	2946	2956

[a] (1:10), (1:100), (1:500), and (1:1000) are mole ratios.

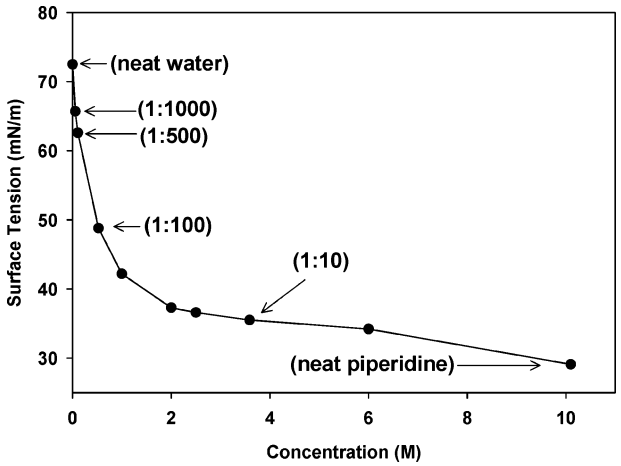

Figure 9. Surface tensions at 22 °C of neat water, neat piperidine, and aqueous piperidine solutions. (1:10), (1:100), (1:500), and (1:1000) are mole ratios between piperidine and H_2O.

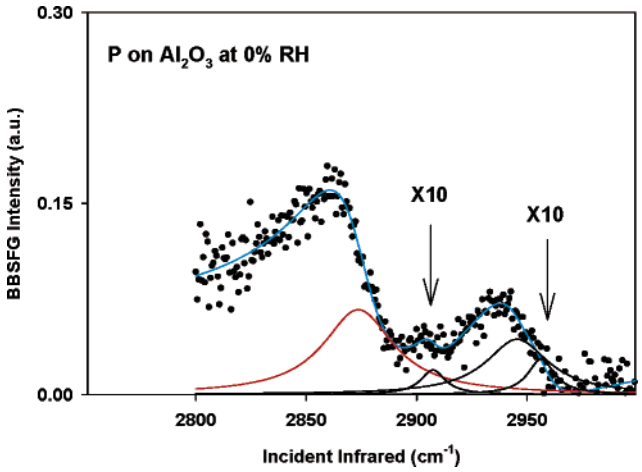

Figure 10. BBSFG spectrum of the air−alumina interface after piperidine adsorption under 0% RH: solid circles, experimental; solid line, Lorentzian fit; blue line, overall fit; red line, probe peak; P, piperidine. ×10 denotes peak magnification.

air−aqueous piperidine interface. This is consistent with the α-CH_2-SS peak at ~2800 cm^{-1} observed in the Raman spectrum of a 1:10 piperidine/H_2O aqueous solution (Figure 7A), which did not show up in the Raman spectra of the aqueous piperidium chloride solutions (Figure 7C and D). Surface tension measurements also support that piperidine is the surface-adsorbed species at the aqueous piperidine surface. As shown in Figure 9, the addition of piperidine (surface tension of neat piperidine is 29.1 mN/m) into water can significantly decrease the surface tension, indicating that piperidine is surface-active. However, the measured surface tension of aqueous piperidium chloride (1: 100 piperidium chloride/H_2O) is 70.3 mN/m, which is very close to the surface tension of pure water (72.5 mN/m). This clearly indicates that piperidium is not as surface-active. Therefore, the surface-adsorbed species of the aqueous piperidine solution is piperidine rather than piperidium.

The BBSFG spectrum of the air−alumina interface after alumina was exposed to the piperidine vapor is shown in Figures 3 and 8D. The spectrum in Figure 8D shows the fit. The peak frequencies are listed in Table 3. The CH_2-SS spectroscopic probe peak is observed at 2875 cm^{-1}. This frequency is almost the same as that of the air−aqueous piperidium chloride interface (frequency at 2874 cm^{-1}) but higher than that of the air−aqueous piperidine interface (frequency at ~2862 cm^{-1}) and the air−neat piperidine interface (frequency at 2854 cm^{-1}). Furthermore, the spectral appearances of the two spectra shown in Figure 8C and D are quite similar to each other. This result strongly suggests that adsorbed piperidine at the alumina surface is protonated. Furthermore, the reaction of HCl vapor with the adsorbed piperidine at the alumina surface was performed. The BBSFG frequency of the probe peak position showed no change after HCl exposure. Therefore, the protonated model, Scenario II in Figure 4 should be the adsorption mechanism of piperidine onto the α-Al_2O_3 (0001) surface.

Scenario II illustrates two different types of surface-adsorbed piperidine species. One type is piperidine protonated by surface-physisorbed water (physisorption) and the other is piperidine directly protonated by surface hydroxyl groups (chemisorption). Though both types of protonation are possible, the pH values of aqueous piperidine solutions as listed in Table 3 indicate that piperidine rather than piperidium is predominant in the aqueous environment. For example, an estimate based on the Henderson−Hasselbalch equation, $\log[piperidine]/[piperidium^+] = pH - pK_a$, reveals that there is only about 20% piperidium even in the most-dilute piperidine solution with a (1:1000) mole ratio between piperidine and H_2O (pK_a of piperidine = 11.07[65,66]). Therefore, if there is a substantial amount of piperidine protonated by H_2O at the alumina surface, there will be a substantial amount of piperidine (not protonated) coexisting at the alumina surface. However, this is not the case since Figure 8D only shows the existence of piperidium at the alumina surface. This means that the majority of the surface-adsorbed species should be piperidine protonated by the alumina surface hydroxyl groups. To further confirm that piperidine can be protonated by the alumina surface hydroxyl groups, the adsorption mechanism was investigated under 0% RH. To perform the experiment under 0% RH, the freshly annealed alumina crystal was first cooled and then kept in lab air (47% RH) for more than

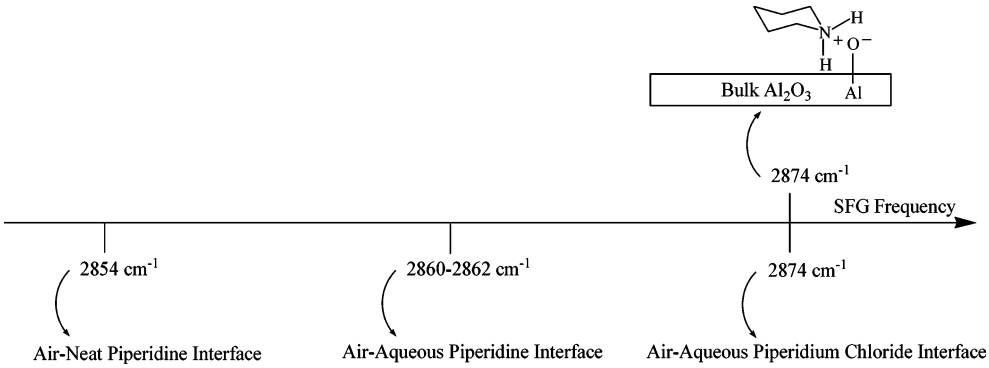

Figure 11. BBSFG probe peak (CH_2-SS) frequencies in the proposed model scenario (the protonation model) and in the reference systems (air−neat piperidine interface, air−aqueous piperidine interface, and air−aqueous piperidium chloride interface)

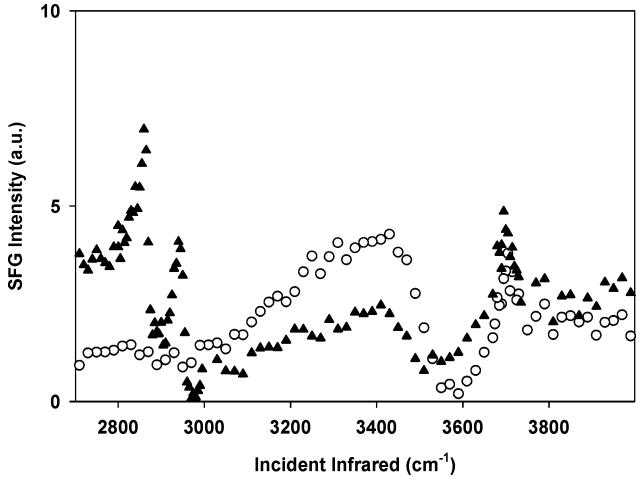

Figure 12. The scanning SFG spectra of the air−solid interface of hydrated α-alumina (0001) surface before (open circles) and after the piperidine adsorption (solid triangles). The alumina crystal was exposed to piperidine vapor for 5 min.

30 min to allow the surface to become hydrated (hydroxylated). As discussed previously, hydrated alumina under ambient conditions is covered by a surface hydroxyl layer and physisorbed water layers. The physisorbed water was removed by placing the alumina crystal into a home-built SFG cell and continuously purging with H_2O-free air for 1 h. The scanning SFG study in the OH stretch region showed that 1 h of purging with H_2O-free air was enough to decrease the SFG intensity in the 3000−3600 cm^{-1} region to the baseline level, indicating the removal of the surface-physisorbed water. Then, piperidine vapor was introduced into the SFG cell to interact with alumina surface hydroxyl groups. The cell was continuously purged by H_2O-free air for 1 h, and then the BBSFG spectrum was recorded in situ. Further purging the SFG cell or introducing additional piperidine vapor into the cell resulted in no spectral variation of the observed BBSFG spectrum shown in Figure 10. Fitting results are listed in Table 3 and indicated the formation of piperidium (piperidine protonated by surface hydroxyl groups only) on the alumina surface. In summary, Figure 11 illustrates the model scenario and the comparison between the alumina surface and the reference systems. Conclusively, piperidine is chemisorbed onto the alumina (0001) surface through protonation by surface hydroxyl groups.

Figure 12 shows the scanning SFG spectra of the alumina surface before and after piperidine adsorption. In addition to the piperidine peaks in the C−H region, two features are observed in the OH region. After the piperidine adsorption, the free OH peak at 3700 cm^{-1} is observed and remains nearly unchanged, except for the slight broadening of its bandwidth. In addition, the hydrogen-bonding network of adsorbed water and the hydrogen-bonded hydroxyls in the 3000−3600 cm^{-1} region are affected by adsorption of piperidine, as revealed by the SFG intensity decrease in this spectral region. The broad OH stretching peak of the SFG spectrum in the 3000−3600 cm^{-1} region contains two major component peaks located at ∼3200 and ∼3450 cm^{-1}. On the basis of the spectral assignments from water cluster studies,[71−73] the 3200 cm^{-1} component is due to the single-donor OH stretch of the hydrogen-bonded surface waters and the 3450 cm^{-1} component is assigned to the double-donor OH stretch of the hydrogen-bonded surface waters. In addition, the 3450 cm^{-1} component also has contribution from the hydrogen-bonded alumina surface hydroxyls.[7,53−57] Fitting results confirmed that the intensity of the two component peaks decreased after the piperidine adsorption. Since piperidine protonation requires the removal of protons from surface hydroxyls, this will result in the decrease of the hydroxyl group surface number density and consequently cause the SFG intensity decrease of the 3450 cm^{-1} component peak.

Conclusion

The interfacial vibrational signature in the C−H stretching region of piperidine at the hydrated α-Al_2O_3 (0001) surface is a sensitive spectroscopic probe revealing the adsorption mechanism of piperidine to the alumina surface. Results indicate that piperidine is protonated by surface hydroxyl groups upon adsorption onto the alumina surface. The O−H stretching region of the alumina surface before and after piperidine adsorption was also investigated, and results revealed the decrease of the surface number density of alumina surface hydroxyl groups.

Acknowledgment. We gratefully acknowledge the National Science Foundation through The Ohio State University Environmental Molecular Science Institute (NSF Grant No. CHE-0089147) and the Department of Energy (DOE-BES Grant No. DE-FG02-04ER15495) for funding this research.

LA0487343

(71) Pribble, R. N.; Zwier, T. S. *Science* **1994**, *265*, 75−79.
(72) Buck, U.; Ettischer, I.; Melzer, M.; Buch, V.; Sadlej, J. *Phys. Rev. Lett.* **1998**, *80*, 2578−2581.
(73) Devlin, J. P.; Sadlej, J.; Buch, V. *J. Phys. Chem. A* **2001**, *105*, 974−983.